Original Article

Magnetic particle imaging of islet transplantation in the liver and under the kidney capsule in mouse models

Ping Wang[1,2], Patrick W. Goodwill[3,4], Prachi Pandit[4], Jeff Gaudet[4], Alana Ross[1], Junfeng Wang[5], Elaine Yu[3], Daniel W. Hensley[3], Timothy C. Doyle[6], Christopher H. Contag[6,7], Steven Conolly[3], Anna Moore[1,2]

[1]Molecular Imaging Laboratory, MGH/MIT/HMS Athinoula A. Martinos Center for Biomedical Imaging, Department of Radiology, Massachusetts General Hospital, Harvard Medical School, Boston, MA, USA; [2]Precision Health Program, Department of Radiology, Michigan State University, East Lansing, MI, USA; [3]Department of Bioengineering, University of California at Berkeley, Berkeley, CA, USA; [4]Magnetic Insight, Inc., Alameda, CA, USA; [5]Gordon Center for Medical Imaging, Department of Radiology, Massachusetts General Hospital, Harvard Medical School, Boston, MA, USA; [6]Department of Pediatrics, Stanford University School of Medicine, Stanford, CA, USA; [7]Institute for Quantitative Health Science and Engineering, Department of Biomedical Engineering, Michigan State University, East Lansing, MI, USA

Correspondence to: Anna Moore, PhD. Precision Health Program, Department of Radiology, Michigan State University, 775 Woodlot Dr., Rm. 3.111, East Lansing, MI 48823, USA. Email: moorea57@msu.edu.

Background: Islet transplantation (Tx) represents the most promising therapy to restore normoglycemia in type 1 diabetes (T1D) patients to date. As significant islet loss has been observed after the procedure, there is an urgent need for developing strategies for monitoring transplanted islet grafts. In this report we describe for the first time the application of magnetic particle imaging (MPI) for monitoring transplanted islets in the liver and under the kidney capsule in experimental animals.

Methods: Pancreatic islets isolated from Papio hamadryas were labeled with superparamagnetic iron oxides (SPIOs) and used for either islet phantoms or Tx in the liver or under the kidney capsule of NOD scid mice. MPI was used to image and quantify islet phantoms and islet transplanted experimental animals post-mortem at 1 and 14 days after Tx. Magnetic resonance imaging (MRI) was used to confirm the presence of labeled islets in the liver and under the kidney capsule 1 day after Tx.

Results: MPI of labeled islet phantoms confirmed linear correlation between the number of islets and the MPI signal (R^2=0.988). Post-mortem MPI performed on day 1 after Tx showed high signal contrast in the liver and under the kidney capsule. Quantitation of the signal supports islet loss over time, which is normally observed 2 weeks after Tx. No MPI signal was observed in control animals. *In vivo* MRI confirmed the presence of labeled islets/islet clusters in liver parenchyma and under the kidney capsule one day after Tx.

Conclusions: Here we demonstrate that MPI can be used for quantitative detection of labeled pancreatic islets in the liver and under the kidney capsule of experimental animals. We believe that MPI, a modality with no depth attenuation and zero background tissue signal could be a suitable method for imaging transplanted islet grafts.

Keywords: Diabetes; pancreatic islet; islet transplantation (Tx); iron oxide nanoparticle; magnetic particle imaging (MPI)

Submitted Jan 16, 2018. Accepted for publication Feb 14, 2018.
doi: 10.21037/qims.2018.02.06
View this article at: http://dx.doi.org/10.21037/qims.2018.02.06

Introduction

Type 1 diabetes (T1D) results from autoimmunity that triggers selective and progressive destruction of pancreatic beta cells. Islet transplantation (Tx) has emerged as the most promising therapy to restore normoglycemia in T1D patients (1). However, even with the success of the Edmonton protocol, the outcome of islet Tx remains suboptimal. According to the most recent report from the Collaborative Islet Transplant Registry, insulin independence 1 year after transplant is achieved in 50% of patients. Unfortunately, islet graft loss causes a decline of independence to below 30% at 5 years (2). Therefore, there is an urgent need for developing strategies and methods for monitoring transplanted islet grafts. Various imaging modalities have been suggested for islet visualization and monitoring after Tx. These include magnetic resonance imaging (MRI) of small paramagnetic iron oxide nanoparticles (SPION)-labeled islets (3-5), PET imaging of ^{18}F-FDG-labeled islets (6,7) and GLP-1-targeted islets (8,9), SPECT imaging of ^{111}In-labeled GLP-1R agonist (10,11), ultrasound imaging (12) and bioluminescence imaging (13). While significant efforts have been made to advance imaging of islet Tx into the clinic, limitations of each modality have so-far hindered wide clinical translation [reviewed in (14)].

Magnetic particle imaging (MPI) is an emerging tracer imaging modality that directly images the magnetization of iron oxide nanoparticles (15), and is specific, sensitive, linearly quantitative, and translatable. MPI has already been utilized for tumor imaging (16), lymph node staging (17), cell tracking (18-21), vascular imaging (22), pulmonary embolism detection using ventilation/perfusion (23), traumatic brain injury (24), and other indications. The technique visualizes the nanoparticle distribution in the sample, and the images can be acquired as both a two-dimensional (2D) projection image (akin to X-ray), as well as in a 3D tomographic image (akin to X-ray CT) (18,25-28). MPI's specificity results from its high image contrast, since magnetic particles serve as the only source for signal and are thus the only visualized element (29). MPI's sensitivity derives from the direct detection of the electronic magnetization of SPIONs, which is 10^8 times larger than the nuclear magnetization of protons seen in MRI (30). This translates to an MPI sensitivity in the hundreds of cells with current hardware and available magnetic nanoparticles (18). MPI's linear quantitation arises from the linear signal change with nanoparticle concentration, which occurs independently of tissue depth, including in the lungs and bone (19). MPI is also safely translatable, as it uses biocompatible iron oxide nanoparticles (31), does not employ ionizing radiation and uses magnetic fields within limits for safe human use (32).

Here we demonstrate, for the first time, applying MPI's specificity, sensitivity, and linear quantification to monitoring transplanted islets in animal models.

Methods

Islet isolation, labeling and Tx

Donor baboon islets (Papio hamadryas, Manheimer Foundation, Homestead, FL, USA) were isolated using Liberase HI (Roche Biochemicals, Indianapolis, IN, USA) digestion as described previously (33). Purity and viability of the islets used for staining, islet phantoms and Tx was >90%.

Isolated islets were labeled with dextran-coated Ferucarbotran SPIOs (VivoTrax, Magnetic Insight Inc., Alameda, CA, USA) at a concentration of 280 µg Fe/mL in CMRL 1066 media for 48 h and washed in PBS prior to Tx. Labeling efficiency was assessed by staining with anti-dextran antibody (Stemcell Technologies, Vancouver, BC, Canada) performed on paraffin-embedded islet sections (34).

Labeled islets [800 labeled islet equivalents (IEQ)] were transplanted into the liver through the portal vein (n=8) or under the left kidney capsule (n=6) of 12-week-old female NOD scid mice. Control animals did not receive islet grafts (n=2).

Imaging of islet phantoms

Islets phantoms comprising of different numbers of labeled islets (25–800 IEQ) in 1% agarose gel were imaged using an MPI scanner (MOMENTUM MPI, Magnetic Insight Inc., Alameda, CA, USA). Fast 2D MPI imaging was performed to quantify the IEQ phantoms. MPI image parameters were a FOV of 4 cm × 6 cm, a 6 T/m selection field gradient, a drive field strength of 20 mT peak amplitude, a 45.0 kHz drive frequency, and an acquisition time of ~10 s. MPI images were reconstructed using x-space reconstruction (18,25-28,35). Quantitative assessment of the IEQ phantoms was performed using the integrated MPI image intensity calibrated against a fiducial marker of known iron concentration (1.1 µg/µL of Fe).

Imaging of transplanted islets

Animals were imaged *in vivo* using MRI at day 1 post Tx and then imaged, postmortem, using MPI. A second cohort was imaged, postmortem, with MPI on day 14 post-Tx. *In vivo* MRI was performed using a 9.4-T Bruker horizontal bore scanner equipped with a Rat Array MRI CryoProbe coil as described previously (34,36). Post-mortem 3D tomographic MPI images were acquired with a FOV of 6 cm × 6 cm × 6 cm, 55 projections, acquisition time of ~10 minutes, with a total imaging time including reconstruction of ~35 minutes. Gradient strength, drive field strength, and drive frequency were unchanged. Anatomic CT reference images were also acquired (CT120, Trifoil Imaging, Northridge, CA, USA). MPI images were co-registered to CT with fiducial markers using VivoQuant Imaging Software (inviCRO, Boston, MA, USA). Iron quantification was performed on the entire CT segmented regions with hand-drawn ROIs of the liver for portal vein injection and kidney for kidney capsule graft.

We need to note that because islets for the calibration curve (islet phantoms) and for Tx came from different batches and were of different quality, we did not include specific estimates of total islet number in the post-mortem groups.

Immunofluorescence of labeled islets and grafts in liver and under the kidney capsule

Frozen 5 µm sections of the kidney and liver were incubated with anti-insulin primary antibody (Santa Cruz Biotechnology, Dallas, TX, USA) and anti-dextran antibody (Stemcells), followed by an FITC-labeled goat anti-mouse secondary IgG (Abcam) and Texas red conjugated goat anti-rabbit secondary IgG (1:100 dilution, Santa Cruz Biotechnology, Santa Cruz, CA, USA). All sections were mounted with a mounting medium containing DAPI and analyzed using fluorescence microscopy.

Statistical analysis

Data are presented as mean ± SD. Statistical comparisons between two groups were evaluated by Student *t*-test and corrected by one-way ANOVA for multiple comparisons using GraphPad Prism 5 (GraphPad Software, Inc., La Jolla, CA, USA). Correlation and linear regression analysis between measured iron content in the phantoms and the number of labeled islets was assessed using GraphPad Prism 5 as well. A value of $P \leq 0.05$ was considered to be statistically significant.

All animal experiments were performed in compliance with institutional guidelines and were approved by the Institutional Animal Care and Use Committee at the Massachusetts General Hospital.

Results

Labeling of pancreatic islets with iron oxide nanoparticles resulted in 95% islet labeling, which was confirmed by staining with anti-dextran antibody (*Figure 1A*). Similar results were obtained in our previous experiments with other iron oxide preparations (3,37). Imaging of labeled islet phantoms revealed direct correlation between the iron content obtained from MPI image analysis and the number of agarose-embedded islets (R^2=0.988, $P<0.0001$) (*Figure 1B,C*).

To ensure the presence of the labeled islets in the liver and under the kidney capsule we performed imaging using conventional MRI. As expected, signal voids representing labeled islets/islet clusters were detected in liver parenchyma (*Figure 2A*) and under the kidney capsule (*Figure 2B*) one day after Tx. These results are in accordance with our previous imaging results showing islets labeled with Feridex or in-house made nanoparticles under the kidney capsule or in the liver (3,38). Immunofluorescence of the frozen tissue sections confirmed the presence of functional islet grafts in the liver and under the kidney capsule of the recipient animals (*Figure 2C*).

Having established the presence of the islets labeled with Ferucarbotran by MRI, we next performed post-mortem MPI co-registered with CT. Animals imaged on days 1 and 14 post Tx showed high signal contrast in the liver and under the kidney capsule (*Figure 3*), and enabled estimation of the iron content at the two transplant locations, confirmed by CT. Since MPI signal is not detectable in the absence of iron oxide nanoparticles, we did not observe any signal in control animals that did not receive the labeled graft (not shown). The images produced by MPI are tomographic and can be presented as multiplanar reconstruction (MPR) and maximum intensity projection (MIP), which are demonstrated in *Figure 3*. Videos showing examples of liver and kidney MIPs 1 and 14 days after Tx are included in the supplementary data (*Figures S1-S4*). MPI images obtained on day 14 after Tx showed visually decreased signal under the kidney capsule (*Figure 3A*) most likely corresponding to the decreased islet mass. This phenomenon is normally observed during the first two

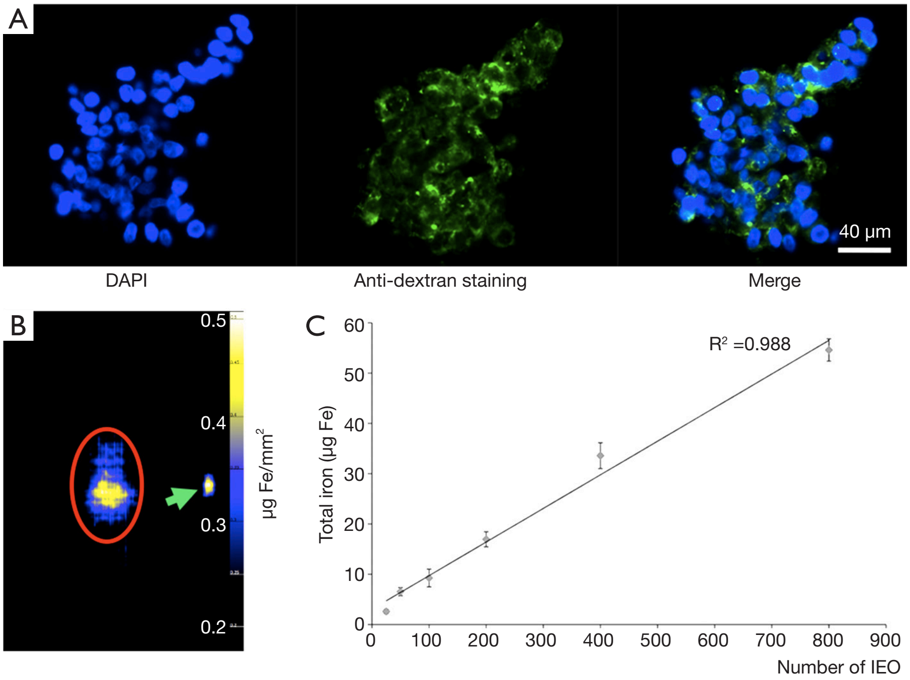

Figure 1 MPI enables linear quantitation of SPIO-labeled islet phantoms. (A) Confirmation of successful SPIO labeling showing anti-dextran immunostaining of islets (green, dextran; blue, DAPI; bar =40 μm). (B) Representative MPI islet phantom image showing an ROI used for quantification (red circle, islet phantom; green arrow, fiducial marker). (C) Measured iron content of the phantoms correlated with the number of labeled islets (R^2=0.988, P<0.0001).

weeks after Tx either under the kidney capsule or in the liver (39,40). Though quantitation of the images confirmed the trend (17.14±3.3 *vs.* 12.2±3.1 μg), it was not statistically significant. We were also able to visualize the tracer released from the dead islets that accumulated in the liver (*Figure 3A*). We did not observe statistical differences between the amount of total iron present in the liver (*Figure 3B*) on days 1 and 14 (15.4±4.5 *vs.* 14.1±3.9 μg). We believe that this was caused by the slow clearance of the iron nanoparticles released from the dead islets. Since MPI signal is not detectable in the absence of iron oxide nanoparticles, we did not observe it in control animals that did not receive the labeled graft (*Figure 3C*).

The sensitivity of MPI made some of the images unusable due to contamination from surgical instruments, animal feed, and feces, which are discussed below.

Discussion

Islet Tx has a potential to restore normoglycemia in T1D patients, who otherwise rely on multiple daily injections of insulin. Clinically, transplanted islets, similar to their endogenous counterparts are significantly more suitable for the human body than exogenously supplied insulin because they have the ability to perfectly time internal insulin release, thus keep blood glucose in normal range.

From existing imaging modalities used for imaging of transplanted islets, MRI seems to be most advanced as these studies have been performed in patients (41,42). However, despite the overall safety of transplanted islets labeled with iron oxide-based contrast agent, image interpretation and quantification of the number of infused islets are ambiguous. As such, the number of infused islets did not correlate with the number of signal voids on MR images. Further, signal voids in MRI, which are produced by iron labeled islets/islet clusters were difficult to distinguish from other low MR signals produced by tissue or artifacts. No doubt negative contrast has contributed to the poor MRI T2* quantitation of the number of infused islets, as noted in prior MRI clinical studies (41,42).

With this study we set the goal to demonstrate quantitative MPI imaging of baboon islets and accurate localization of islets with a co-registered CT, as well as to describe possible challenges for future *in vivo* studies.

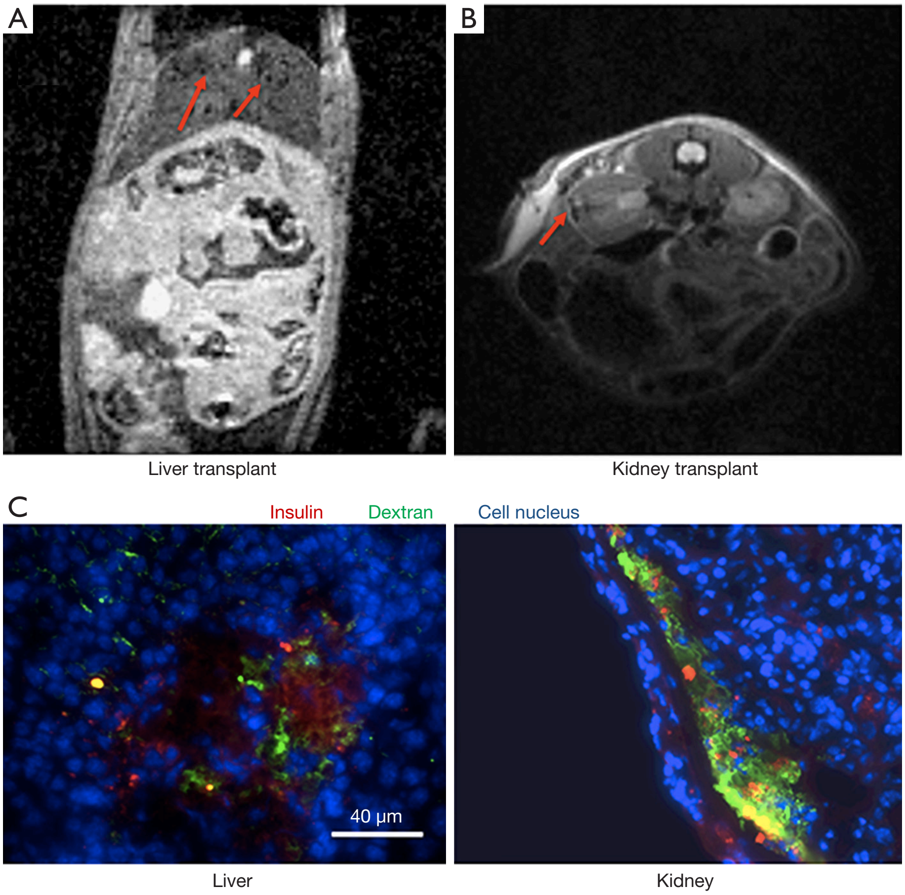

Figure 2 Localization of transplanted islets on day 1. (A) MRI confirms transplant presence in the liver and (B) under the kidney capsule. (C) Immunofluorescence of the frozen tissue sections confirmed the presence of functional islet grafts in the liver and under the kidney capsule (red, insulin; green, dextran; blue, DAPI; bar =40 µm). Arrows indicate islets grafts in the liver (A) and under the kidney capsule (B).

In contrast to MRI, MPI enables quantification of islet number (18). In *Figure 1*, we demonstrate the linearity of MPI signal by measuring six different IEQ phantoms. The quantification shows the MPI signal increases linearly with the number of labeled IEQs (R^2=0.988). *In vivo*, the quantitation could be used to monitor the change in MPI signal over time as a marker of graft deterioration. In this study we used 800 IEQ per transplant to establish the feasibility of detection *in vivo*. In the future studies we will use smaller number of islets based on the fact that 100–300 islets were easily detectable in the phantom study. However, there are several considerations that have to be taken into account. In the case of MRI, which has low sensitivity, iron is only detected in its compartmentalized form in islet cells/islet clusters. Following islet death, the iron oxide tracer is released in the interstitium where its local concentration is too low to be detected by MRI. The released nanoparticles are then taken up and broken down by Kupffer cells in the liver over the course of several weeks (38). In the case of MPI with much higher sensitivity, if the released iron nanoparticles have not been cleared, they are detected even if outside of the islet cells. Because of the short timeline of our experiment, signal decreases were not obvious between days 1 and 14 following liver Tx. In the future, it would be beneficial to use iron oxide nanoparticles with fast clearance. In spite of these issues, unlike MRI, MPI allows for the detection of the signal coming specifically from the islets immediately after Tx as magnetic nanoparticles serve as the only source for that signal. The specificity of MPI is also demonstrated in *Figure 3*, where in the case of the kidney transplant it was possible to distinguish between the signals from the kidney and from the liver where the released nanoparticles accumulated. This means that if the animal is monitored over time, MPI could provide information on

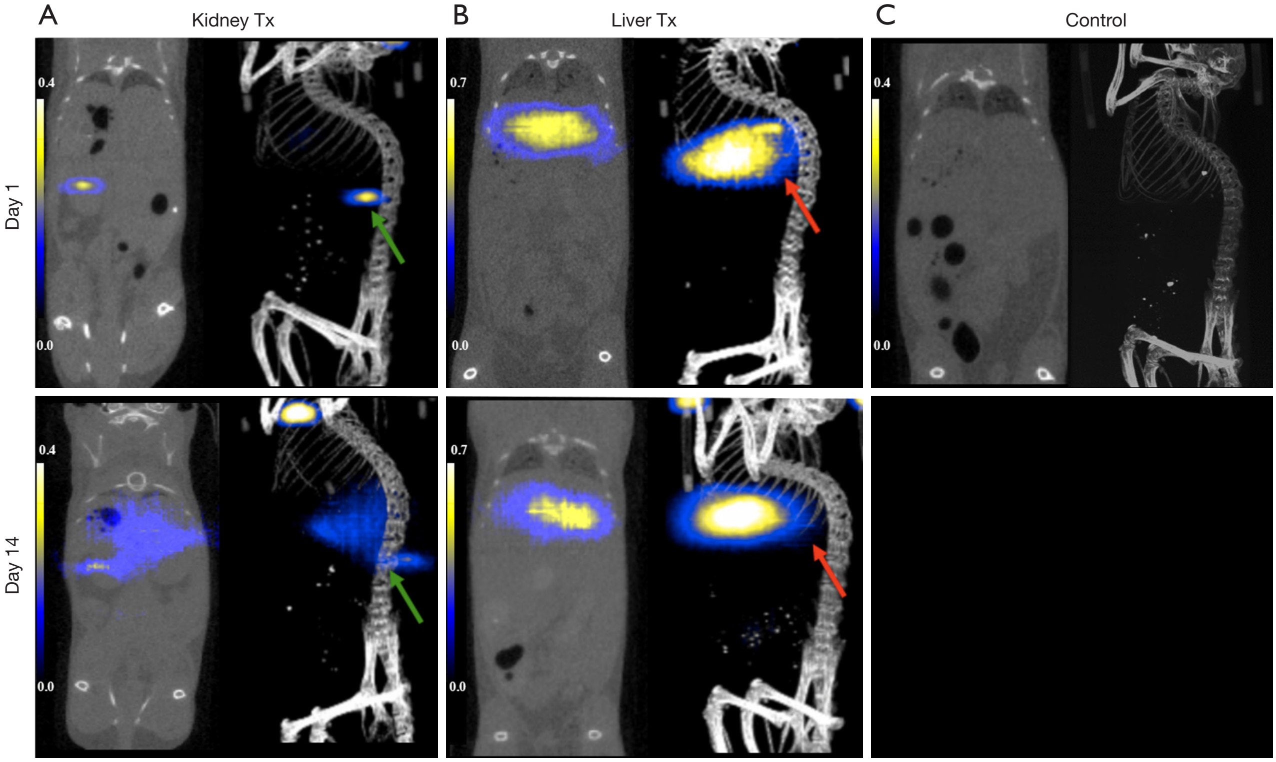

Figure 3 MPI confirms 3D spatial Tx location and allows for longitudinal quantification (in all images: left, coronal; right, sagittal). (A) MPI of the islets transplanted under the kidney capsule (green arrows). (B) MPI of the islets transplanted in the liver (red arrows) (C) No signal was observed in the control. Bar = μgFe/mm^2.

iron metabolism and biodistribution after release from the islets.

As seen above, the sensitivity of MPI for detecting small quantities of iron presented us with new challenges. A number of animals produced unusable images due to the use of metal surgical instruments, contaminated feed, a feces signal, and contaminated paper products. We noticed that some initial specimens produced signal at surgical sites (*Figure S5*) that we attributed to the microscopic shavings shed from metal instruments used in Tx, which we remedied in later animals. We also noted that some animals produced significant signal in their gut attributed to a significant amount of iron in mouse chow. Later animals were fed a laxative, which demonstrably eliminated the feces signal. Last, during imaging, we observed background signal from the use of recycled paper products used to position the animals, which we rectified in later images.

Beyond islet tracking, MPI is more widely applicable to research developing treatments for diabetes such as novel stem cell replacement therapies (43,44), and understanding islet rejection. For example, studies that have recently advanced to phase I trials (43,44) successfully demonstrate application of human embryonic stem cell (hESC)-derived pancreatic progenitors for restoring normoglycemia. Protocols describing generation of insulin-producing beta-cells by differentiation of human pluripotent stem cells (hPSCs) along the pancreatic lineage have also been developed and are now widely available for diabetes researches (45). Regardless of the source of beta-cells used for Tx there remains a need to detect and monitor these transplants over time in experimental animals and in humans. MPI could also be used for development and testing of drugs for islet protection. As magnetic nanoparticles can be synthesized to carry a payload, islets could also be treated and labeled at the same time prior to Tx. In our previous studies we have already shown protective effect of theranostic magnetic nanoparticles carrying siRNA directed towards genes responsible for islet damage (34,46). We believe that MPI could assist researcher and clinicians in detecting grafts from various sources and monitoring them over time. Finally, as islet Tx surgeons try to find sites more suitable for islet survival (47,48), the approach described above could assist in establishing those new sites.

Here we have shown that MPI has great promise for visualizing, quantifying, and monitoring islet Tx. The lessons learned in these post mortem animals are now being applied as we work to translate these initial results into *in vivo* islet tracking studies. We believe that MPI could play an important role in monitoring the grafts, both by directly imaging of the graft itself, as well as through indirect measurements of signal in RES organs such as the liver.

Acknowledgements

None.

Footnote

Conflicts of Interest: Dr. Patrick Goodwill, Prof. Steven Conolly, Dr. Daniel Hensley, Dr. Prachi Pandit and Dr. Jeff Gaudet hold equity interest in Magnetic Insight, Inc. In addition, Dr. Goodwill, Dr. Hensley, Dr. Pandit, and Dr. Gaudet receive income from Magnetic Insight, Inc.

Ethical Statement: All animal experiments were performed in compliance with institutional guidelines and were approved by the Institutional Animal Care and Use Committee at the Massachusetts General Hospital (No. 2005N000066).

References

1. McCall M, Shapiro AM. Update on islet transplantation. Cold Spring Harb Perspect Med 2012;2:a007823.
2. Collaborative Islet Transplant Registry, Ninth Annual Report. Rockville MD: National Institute of Diabetes and Digestive and Kidney Diseases National Institutes of Health US Department of Health and Human Services 2016, December 8, 2016.
3. Evgenov NV, Medarova Z, Dai G, Bonner-Weir S, Moore A. In vivo imaging of islet transplantation. Nat Med 2006;12:144-8.
4. Medarova Z, Evgenov NV, Dai G, Bonner-Weir S, Moore A. In vivo multimodal imaging of transplanted pancreatic islets. Nat Protoc 2006;1:429-35.
5. Jirak D, Kriz J, Herynek V, Andersson B, Girman P, Burian M, Saudek F, Hajek M. MRI of transplanted pancreatic islets. Magn Reson Med 2004;52:1228-33.
6. Eich T, Eriksson O, Lundgren T. Visualization of early engraftment in clinical islet transplantation by positron-emission tomography. N Engl J Med 2007;356:2754-5.
7. Eriksson O, Eich T, Sundin A, Tibell A, Tufveson G, Andersson H, Felldin M, Foss A, Kyllonen L, Langstrom B, Nilsson B, Korsgren O, Lundgren T. Positron emission tomography in clinical islet transplantation. Am J Transplant 2009;9:2816-24.
8. Wu Z, Liu S, Hassink M, Nair I, Park R, Li L, Todorov I, Fox JM, Li Z, Shively JE, Conti PS, Kandeel F. Development and Evaluation of 18F-TTCO-Cys40-Exendin-4: A PET Probe for Imaging Transplanted Islets. J Nucl Med 2013;54:244-51.
9. Wu Z, Todorov I, Li L, Bading JR, Li Z, Nair I, Ishiyama K, Colcher D, Conti PE, Fraser SE, Shively JE, Kandeel F. In vivo imaging of transplanted islets with 64Cu-DO3A-VS-Cys40-Exendin-4 by targeting GLP-1 receptor. Bioconjug Chem 2011;22:1587-94.
10. Christ E, Wild D, Forrer F, Brandle M, Sahli R, Clerici T, Gloor B, Martius F, Maecke H, Reubi JC. Glucagon-like peptide-1 receptor imaging for localization of insulinomas. J Clin Endocrinol Metab 2009;94:4398-405.
11. Pattou F, Kerr-Conte J, Wild D. GLP-1-receptor scanning for imaging of human beta cells transplanted in muscle. N Engl J Med 2010;363:1289-90.
12. Sakata N, Goto M, Gumpei Y, Mizuma M, Motoi F, Satomi S, Unno M. Intraoperative ultrasound examination is useful for monitoring transplanted islets: a case report. Islets 2012;4:339-42.
13. Chen X, Zhang X, Larson CS, Baker MS, Kaufman DB. In vivo bioluminescence imaging of transplanted islets and early detection of graft rejection. Transplantation 2006;81:1421-7.
14. Wang P, Medarova Z, Moore A. Molecular imaging: a promising tool to monitor islet transplantation. J Transplant 2011;2011:202915.
15. Gleich B, Weizenecker J. Tomographic imaging using the nonlinear response of magnetic particles. Nature 2005;435:1214-7.
16. Yu EY, Bishop M, Zheng B, Ferguson RM, Khandhar AP, Kemp SJ, Krishnan KM, Goodwill PW, Conolly SM. Magnetic Particle Imaging: A Novel in Vivo Imaging Platform for Cancer Detection. Nano Lett 2017;17:1648-54.
17. Gräfe K, Sattel TF, Lüdtke-Buzug K, Finas D, Borgert J, Buzug TM. Magnetic-Particle-Imaging for Sentinel Lymph Node Biopsy in Breast Cancer. In: Buzug T, Borgert J. editors. Magnetic Particle Imaging. Springer Proceedings in Physics. Berlin, Heidelberg: Springer, 2012.

18. Zheng B, Vazin T, Goodwill PW, Conway A, Verma A, Saritas EU, Schaffer D, Conolly SM. Magnetic Particle Imaging tracks the long-term fate of in vivo neural cell implants with high image contrast. Sci Rep 2015;5:14055.
19. Zheng B, von See MP, Yu E, Gunel B, Lu K, Vazin T, Schaffer DV, Goodwill PW, Conolly SM. Quantitative Magnetic Particle Imaging Monitors the Transplantation, Biodistribution, and Clearance of Stem Cells In Vivo. Theranostics 2016;6:291-301.
20. Bulte JW, Walczak P, Gleich B, Weizenecker J, Markov DE, Aerts HC, Boeve H, Borgert J, Kuhn M. MPI cell tracking: what can we learn from MRI? Proc SPIE Int Soc Opt Eng 2011;7965:79650z.
21. Bulte JW, Walczak P, Janowski M, Krishnan KM, Arami H, Halkola A, Gleich B, Rahmer J. Quantitative "Hot Spot" imaging of transplanted stem cells using superparamagnetic tracers and Magnetic Particle Imaging (MPI). Tomography 2015;1:91-7.
22. Khandhar AP, Keselman P, Kemp SJ, Ferguson RM, Goodwill PW, Conolly SM, Krishnan KM. Evaluation of PEG-coated iron oxide nanoparticles as blood pool tracers for preclinical magnetic particle imaging. Nanoscale 2017;9:1299-306.
23. Zhou XY, Jeffris KE, Yu EY, Zheng B, Goodwill PW, Nahid P, Conolly SM. First in vivo magnetic particle imaging of lung perfusion in rats. Phys Med Biol 2017;62:3510-22.
24. Orendorff R, Peck AJ, Zheng B, Shirazi SN, Matthew Ferguson R, Khandhar AP, Kemp SJ, Goodwill P, Krishnan KM, Brooks GA, Kaufer D, Conolly S. First in vivo traumatic brain injury imaging via magnetic particle imaging. Phys Med Biol 2017;62:3501-9.
25. Knopp T, Sattel TF, Biederer S, Rahmer J, Weizenecker J, Gleich B, Borgert J, Buzug TM. Model-based reconstruction for magnetic particle imaging. IEEE Trans Med Imaging 2010;29:12-8.
26. Konkle JJ, Goodwill PW, Carrasco-Zevallos OM, Conolly SM. Projection reconstruction magnetic particle imaging. IEEE Trans Med Imaging 2013;32:338-47.
27. Konkle JJ, Goodwill PW, Hensley DW, Orendorff RD, Lustig M, Conolly SM. A convex cormulation for magnetic particle imaging x-space reconstruction. PLoS One 2015;10:e0140137.
28. Konkle JJ, Goodwill PW, Saritas EU, Zheng B, Lu K, Conolly SM. Twenty-fold acceleration of 3D projection reconstruction MPI. Biomed Tech (Berl) 2013;58:565-76.
29. Panagiotopoulos N, Duschka RL, Ahlborg M, Bringout G, Debbeler C, Graeser M, Kaethner C, Ludtke-Buzug K, Medimagh H, Stelzner J, Buzug TM, Barkhausen J, Vogt FM, Haegele J. Magnetic particle imaging: current developments and future directions. Int J Nanomedicine 2015;10:3097-114.
30. Goodwill P, Tamrazian A, Croft L, Lu C, Johnson E, Pidaparthi R, Ferguson R, Khandhar A, Krishnan K, Connoly S. Ferrohydrodynamic relaxometry for magnetic particle imaging. Appl Phys Lett 2011;98:262502.
31. Goodwill PW, Saritas EU, Croft LR, Kim TN, Krishnan KM, Schaffer DV, Conolly SM. X-space MPI: magnetic nanoparticles for safe medical imaging. Adv Mater 2012;24:3870-7.
32. Saritas EU, Goodwill PW, Zhang GZ, Conolly SM. Magnetostimulation limits in magnetic particle imaging. IEEE Trans Med Imaging 2013;32:1600-10.
33. Wang P, Schuetz C, Vallabhajosyula P, Medarova Z, Tena A, Wei L, Yamada K, Deng S, Markmann JF, Sachs DH, Moore A. Monitoring of allogeneic islet grafts in nonhuman primates using MRI. Transplantation 2015;99:1574-81.
34. Wang P, Yigit MV, Medarova Z, Wei L, Dai G, Schuetz C, Moore A. Combined small interfering RNA therapy and in vivo magnetic resonance imaging in islet transplantation. Diabetes 2011;60:565-71.
35. Lu K, Goodwill PW, Saritas EU, Zheng B, Conolly SM. Linearity and shift invariance for quantitative magnetic particle imaging. IEEE Trans Med Imaging 2013;32:1565-75.
36. Wang P, Schuetz C, Ross A, Dai G, Markmann JF, Moore A. Immune rejection after pancreatic islet cell transplantation: in vivo dual contrast-enhanced MR imaging in a mouse model. Radiology 2013;266:822-30.
37. Medarova Z, Vallabhajosyula P, Tena A, Evgenov N, Pantazopoulos P, Tchipashvili V, Weir G, Sachs D, Moore A. In vivo imaging of autologous islet grafts in the liver and under the kidney capsule in non-human primates. Transplantation 2009;87:1659-66.
38. Evgenov NV, Medarova Z, Pratt J, Pantazopoulos P, Leyting S, Bonner-Weir S, Moore A. In vivo imaging of immune rejection in transplanted pancreatic islets. Diabetes 2006;55:2419-28.
39. Davalli AM, Scaglia L, Zangen DH, Hollister J, Bonner-Weir S, Weir GC. Vulnerability of islets in the immediate posttransplantation period. Dynamic changes in structure and function. Diabetes 1996;45:1161-7.
40. Chang EN, Scudamore CH, Chung SW. Transplantation: focus on kidney, liver and islet cells. Can J Surg 2004;47:122-9.

41. Saudek F, Jirak D, Girman P, Herynek V, Dezortova M, Kriz J, Peregrin J, Berkova Z, Zacharovova K, Hajek M. Magnetic resonance imaging of pancreatic islets transplanted into the liver in humans. Transplantation 2010;90:1602-6.
42. Toso C, Vallee JP, Morel P, Ris F, Demuylder-Mischler S, Lepetit-Coiffe M, Marangon N, Saudek F, James Shapiro AM, Bosco D, Berney T. Clinical magnetic resonance imaging of pancreatic islet grafts after iron nanoparticle labeling. Am J Transplant 2008;8:701-6.
43. Kroon E, Martinson LA, Kadoya K, Bang AG, Kelly OG, Eliazer S, Young H, Richardson M, Smart NG, Cunningham J, Agulnick AD, D'Amour KA, Carpenter MK, Baetge EE. Pancreatic endoderm derived from human embryonic stem cells generates glucose-responsive insulin-secreting cells in vivo. Nat Biotechnol 2008;26:443-52.
44. Rezania A, Bruin JE, Riedel MJ, Mojibian M, Asadi A, Xu J, Gauvin R, Narayan K, Karanu F, O'Neil JJ, Ao Z, Warnock GL, Kieffer TJ. Maturation of human embryonic stem cell-derived pancreatic progenitors into functional islets capable of treating pre-existing diabetes in mice. Diabetes 2012;61:2016-29.
45. Van Hoof D, Liku ME. Directed differentiation of human pluripotent stem cells along the pancreatic endocrine lineage. Methods Mol Biol 2013;997:127-40.
46. Wang P, Yigit MV, Ran C, Ross A, Wei L, Dai G, Medarova Z, Moore A. A theranostic small interfering RNA nanoprobe protects pancreatic islet grafts from adoptively transferred immune rejection. Diabetes 2012;61:3247-54.
47. Perez VL, Caicedo A, Berman DM, Arrieta E, Abdulreda MH, Rodriguez-Diaz R, Pileggi A, Hernandez E, Dubovy SR, Parel JM, Ricordi C, Kenyon NM, Kenyon NS, Berggren PO. The anterior chamber of the eye as a clinical transplantation site for the treatment of diabetes: a study in a baboon model of diabetes. Diabetologia 2011;54:1121-6.
48. Ali Y, Diez J, Selander L, Zheng X, Edlund H, Berggren PO. The anterior chamber of the eye is a transplantation site that supports and enables visualisation of beta cell development in mice. Diabetologia 2016;59:1007-11.

Cite this article as: Wang P, Goodwill PW, Pandit P, Gaudet J, Ross A, Wang J, Yu E, Hensley DW, Doyle TC, Contag CH, Conolly S, Moore A. Magnetic particle imaging of islet transplantation in the liver and under the kidney capsule in mouse models. Quant Imaging Med Surg 2018;8(2):114-122. doi: 10.21037/qims.2018.02.06

Supplementary

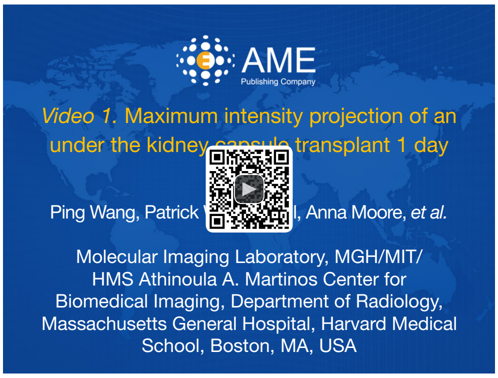
AME
Publishing Company

Video 1. Maximum intensity projection of an
under the kidney capsule transplant 1 day

Ping Wang, Patrick l, Anna Moore, *et al.*

Molecular Imaging Laboratory, MGH/MIT/
HMS Athinoula A. Martinos Center for
Biomedical Imaging, Department of Radiology,
Massachusetts General Hospital, Harvard Medical
School, Boston, MA, USA

Figure S1 Maximum intensity projection of an under the kidney capsule transplant 1 day after Tx (49).
Available online: http://www.asvide.com/article/view/23695

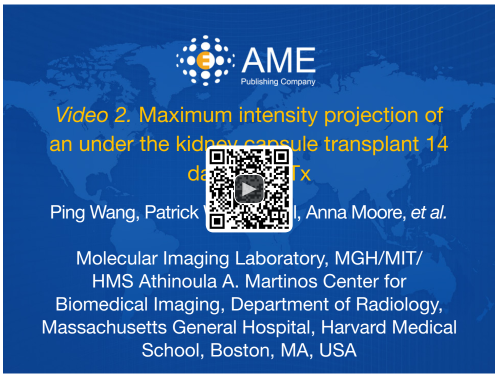
AME
Publishing Company

Video 2. Maximum intensity projection of
an under the kidney capsule transplant 14
da Tx

Ping Wang, Patrick l, Anna Moore, *et al.*

Molecular Imaging Laboratory, MGH/MIT/
HMS Athinoula A. Martinos Center for
Biomedical Imaging, Department of Radiology,
Massachusetts General Hospital, Harvard Medical
School, Boston, MA, USA

Figure S2 Maximum intensity projection of an under the kidney capsule transplant 14 days after Tx (50).
Available online: http://www.asvide.com/article/view/23696

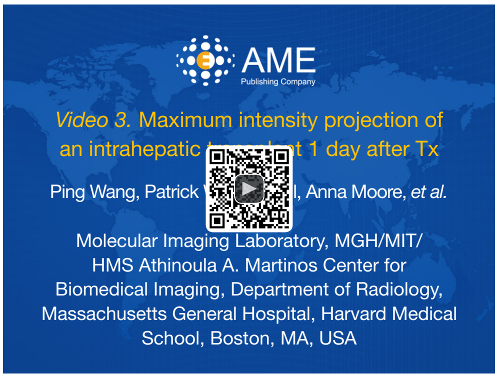
AME
Publishing Company

Video 3. Maximum intensity projection of
an intrahepatic t 1 day after Tx

Ping Wang, Patrick l, Anna Moore, *et al.*

Molecular Imaging Laboratory, MGH/MIT/
HMS Athinoula A. Martinos Center for
Biomedical Imaging, Department of Radiology,
Massachusetts General Hospital, Harvard Medical
School, Boston, MA, USA

Figure S3 Maximum intensity projection of an intrahepatic transplant 1 day after Tx (51).
Available online: http://www.asvide.com/article/view/23697

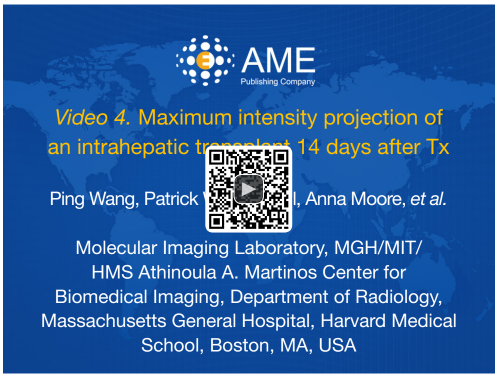
AME
Publishing Company

Video 4. Maximum intensity projection of
an intrahepatic transplant 14 days after Tx

Ping Wang, Patrick l, Anna Moore, *et al.*

Molecular Imaging Laboratory, MGH/MIT/
HMS Athinoula A. Martinos Center for
Biomedical Imaging, Department of Radiology,
Massachusetts General Hospital, Harvard Medical
School, Boston, MA, USA

Figure S4 Maximum intensity projection of an intrahepatic transplant 14 days after Tx (52).
Available online: http://www.asvide.com/article/view/23698

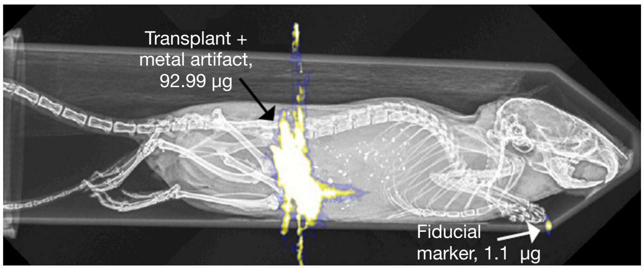

Figure S5 Non-specific signal at surgical site attributed to the microscopic shavings shed from metal instruments.

References

49. Wang P, Goodwill PW, Pandit P, Gaudet J, Ross A, Wang J, Yu E, Hensley DW, Doyle TC, Contag CH, Conolly S, Moore A. Maximum intensity projection of an under the kidney capsule transplant 1 day after Tx. Asvide 2018;5:304. Available online: http://www.asvide.com/article/view/23695
50. Wang P, Goodwill PW, Pandit P, Gaudet J, Ross A, Wang J, Yu E, Hensley DW, Doyle TC, Contag CH, Conolly S, Moore A. Maximum intensity projection of an under the kidney capsule transplant 14 days after Tx. Asvide 2018;5:305. Available online: http://www.asvide.com/article/view/23696
51. Wang P, Goodwill PW, Pandit P, Gaudet J, Ross A, Wang J, Yu E, Hensley DW, Doyle TC, Contag CH, Conolly S, Moore A. Maximum intensity projection of an intrahepatic transplant 1 day after Tx. Asvide 2018;5:306. Available online: http://www.asvide.com/article/view/23697
52. Wang P, Goodwill PW, Pandit P, Gaudet J, Ross A, Wang J, Yu E, Hensley DW, Doyle TC, Contag CH, Conolly S, Moore A Maximum intensity projection of an intrahepatic transplant 14 days after Tx. Asvide 2018;5:307. Available online: http://www.asvide.com/article/view/23698